HHS Public Access

Author manuscript

Cancer Res. Author manuscript; available in PMC 2018 November 15.

Published in final edited form as:

Cancer Res. 2017 November 15; 77(22): 6330–6339. doi:10.1158/0008-5472.CAN-17-2043.

Genome-wide CRISPR screen for essential cell growth mediators in mutant KRAS colorectal cancers

Edwin H. Yau[1,2,3], **Indrasena Reddy Kummetha**[1], **Gianluigi Lichinchi**[1], **Rachel Tang**[1], **Yunlin Zhang**[1], and **Tariq M. Rana**[1,3]

[1]Department of Pediatrics and Institute for Genomic Medicine, University of California San Diego School of Medicine, 9500 Gilman Drive MC 0762, La Jolla, California, 92093, USA

[2]Division of Hematology-Oncology, Department of Internal Medicine, University of California San Diego School of Medicine, La Jolla, CA 92037

[3]Solid Tumor Therapeutics Program, Moores Cancer Center, University of California, San Diego, 3855 Health Sciences Drive, La Jolla, CA 92093

Abstract

Targeting mutant KRAS signaling pathways continues to attract attention as a therapeutic strategy for KRAS-driven tumors. In this study, we exploited the power of the CRISPR-Cas9 system to identify genes affecting the tumor xenograft growth of human mutant KRAS colorectal cancers ($KRAS^{MUT}$ CRC). Using pooled lentiviral single guide RNA libraries, we conducted a genome-wide loss-of-function genetic screen in an isogenic pair of human CRC cell lines harboring mutant or wild-type KRAS. The screen identified novel and established synthetic enhancers or synthetic lethals for $KRAS^{MUT}$ CRC, including targetable metabolic genes. Notably, genetic disruption or pharmacologic inhibition of the metabolic enzymes NAD kinase (NADK) or ketohexokinase (KHK) were growth inhibitory in vivo. Additionally, the chromatin remodeling protein INO80C was identified as a novel tumor suppressor in $KRAS^{MUT}$ colorectal and pancreatic tumor xenografts. Our findings define a novel targetable set of therapeutic targets for $KRAS^{MUT}$ tumors.

Keywords

KRAS; CRISPR-Cas9; genome-wide; NADK; KHK; INO80C; cancer metabolism

INTRODUCTION

The *RAS* family of oncogenes (*KRAS*, *NRAS*, and *HRAS*) is the target of intense research for two reasons: the crucial role of mutant RAS proteins in tumorigenesis and the continued unmet need for therapeutic options for *RAS*-mutated human cancers. *RAS* is the most frequently mutated oncogenic driver of human cancer, and *KRAS* is mutated in about 20% of all human cancers, including some of the most lethal. Because of the historic difficulty in targeting *RAS*, genomic screening using synthetic lethal/enhancing approaches has become

*Corresponding and Lead Contact: T.M.R. (trana@ucsd.edu).

Conflict of Interest: The authors declare no competing financial interests

an attractive method to identify more tractable therapeutic targets and to further understand *RAS* biology. The approach identifies genetic targets whose disruption does not normally affect survival but becomes lethal/enhancing in the presence of an activating *RAS* mutation (1,2).

Functional genomic screens have been revolutionized by application of the gene-specific editing technology of clustered regularly interspaced short palindrome repeats (CRISPR) and CRISPR-associated protein 9 (Cas9) system, which allows efficient and specific genome engineering in mammalian cells (3–5). By targeting the Cas9 nuclease gene using specific single guide RNAs (sgRNAs) and inducing targeted double-strand DNA breaks that are repaired by error-prone non-homologous end joining, insertion or deletion mutations can be introduced into 5′ exons of coding genes, resulting in loss-of-function mutants. A number of groups have used pooled oligonucleotide array synthesis to generate and validate large sgRNA libraries for genome-wide loss-of-function (knockout) studies (6–11).

In cell culture models, genome-wide CRISPR-Cas9 knockout screens have revealed that *KRAS* wild-type (*KRAS*^{WT}) and mutant (*KRAS*^{MUT}) tumor cells show differential dependencies on downstream MAPK signaling members and adapters, and that *KRAS*^{MUT} tumors are highly dependent on mitochondrial oxidative phosphorylation (7,10). To extend our knowledge of the genetic vulnerabilities of *KRAS*^{MUT} tumors to the in vivo setting, we performed a pooled CRISPR-Cas9 knockout screen of tumor xenografts using an isogenic pair of human colorectal cancer (CRC) cell lines carrying wild-type or mutant *KRAS*. We identified gene knockouts that conferred selective beneficial or detrimental effects in the context of *KRAS* activation, including multiple metabolic vulnerabilities, highlighting the therapeutic potential of targeting cancer metabolism in *KRAS*^{MUT} tumors. Using a secondary validation sgRNA library, we additionally identified a novel *KRAS*-dependent tumor suppressor gene in *KRAS*$^{WT/MUT}$ CRC and pancreatic adenocarcinoma (PDAC) isogenic xenografts.

MATERIALS AND METHODS

Cell Lines and Culture

The paired isogenic CRC cell lines HCT116 *KRAS*$^{WT/-}$, HCT116 *KRAS*$^{WT/G13D}$, DLD-1 *KRAS*$^{WT/-}$, and DLD-1 *KRAS*$^{WT/G13D}$ (abbreviated to ^{WT} and ^{MUT}) were kind gifts from Dr. Bert Vogelstein (Johns Hopkins University, Baltimore, MD). Capan-2, SW1990, H348, and H441 cells were from the ATCC (Manassas, VA). All cell lines were cultured in DMEM (Invitrogen) with 10% fetal bovine serum (FBS; Invitrogen) and 1% penicillin/streptomycin (Invitrogen). HCT116 cell lines were validated by PCR amplification and Sanger sequencing to confirm the mutation at the genomic level. Strict bio-banking procedures were followed and cells were tested for contamination, including mycoplasma. HCT116-dCas9, DLD-1-dCas9, H358-dCas9, and Capan-2-dCas9 cell lines were generated by lentiviral transduction with lentiCas9-Blast (Addgene # 52962) and selection with 10 μg/mL of blasticidin.

Pooled Library Amplification and Viral Production

We followed previously published protocols of screens using the GeCKO library, as developed by the Zhang lab, with slight modifications. The human GeCKO v2 A library pooled plasmid (lentiCRISPR v2) was obtained from Addgene (cat # 1000000048) and amplified according to the recommended protocols by electroporation in Lucigen Endura electrocompetent cells. For the secondary focused validation sgRNA library, oligonucleotide pools (CustomArray) were obtained with variable 20 bp sgRNA sequences flanked by universal PCR primers (74 bp total synthesized sequence, see Supplementary Experimental Procedures for full sequences). Full-length oligonucleotides were amplified by PCR using Q5 HiFi polymerase (New England Biolabs) and size-selected on 2% agarose gels. PCR inserts were cloned into BsmBI-digested lentiGuide-Puro (Addgene # 52963) using Gibson assembly (New England Biolabs), transformed into Endura electrocompetent cells, and amplified similarly to the GeCKO library. 293FT cells were resuspended in DMEM and co-transfected with 12 μg of the hGeCKO plasmid library or secondary validation mini-pool, 9 μg psPAX2 vector, and 6 μg pMD2.G vector in 10 cm plates using 48 μL of PLUS reagent (Invitrogen 11514-015) and 60 μL of Lipofectamine in Opti-MEM medium. The medium was aspirated after 6 h and replaced with fresh DMEM/10% FBS. The supernatant was harvested after 60 h, centrifuged at 3000 rpm at 4°C for 10 min, filtered through a 0.45 μm low protein binding membrane (Millipore), and concentrated using an Amicon Ultra-15 Centrifugal Filter (Millipore) for 40 min at 4°C at 4000 rpm. The virus was then aliquoted and frozen at −80°C.

Pooled Library Transduction

A functional virus titer was obtained by measuring puromycin resistance after transduction via spinfection, as previous published (8). A titer resulting in 20%–40% of cells surviving puromycin selection was calculated to correspond to a MOI of 0.2–0.5 and a single infection percentage of 77%–89%. For the genome-wide screen, duplicate transductions with 1.6×10^8 cells each were infected at a MOI ~0.2 for coverage of ~500×. For the secondary validation mini-pools, triplicate transductions with 1.2×10^7 cells each were infected at a MOI ~0.2 for coverage of ~1000×. Transduced cells were selected with 2 μg/mL puromycin for 7 days. Cells were passaged with a seeding density of 3×10^7 cells for the genome-wide screen and 1×10^7 cells for the secondary mini-pool screen at each passage to maintain library representation.

Mouse Xenografts

All animal studies were approved by the UC San Diego Institutional Animal Care and Use Committee. HCT116 cells transduced with the GeCKO library or HCT116-dCas9 cells and Capan-2-dCas9 transduced with the secondary mini-library or individual sgRNA constructs were washed with PBS, resuspended in 300 μL of PBS and Matrigel (1:1 ratio), and injected subcutaneously into the flanks of nude mice (NU/J, Jackson Labs). For the primary GeCKO screen and secondary mini-library screens, 3×10^7 cells were injected per mouse and groups of 3 mice were injected per transduction replicate per cell line. After 14 days, mice were euthanized and the tumors excised and stored in RNAlater (Qiagen) solution. For individual sgRNA experiments, 1.5×10^6 HCT116, DLD-1, H358, or Capan-2 tumor cells were

resuspended in PBS:Matrigel (1:1) and injected into the flanks of nude mice (3–4 mice per sgRNA, 6–8 mice per gene targeted). Tumor dimensions were measured with Vernier calipers for 24 days, and volumes (mm^3) were calculated as (0.5 × width) × ($height^2$).

Small Molecule Inhibitor Treatment

Nude mice were injected with HCT116 tumor cells as above. After xenografts were palpable (~7 days after injection), animals were injected intraperitoneally with 100 μL of vehicle, thionicotinamide (Spectrum; 100 mg/kg body weight) in 1% DMSO, or KHK inhibitor (Calbiochem or synthesized according to published methods (12); 25 mg/kg) in PBS. Injections were repeated every other day for 14 days (7 doses total). Tumor dimensions were measured with Vernier calipers, and volumes (mm^3) were calculated as (0.5 × width) × ($height^2$).

sgRNA Library Quantification by Deep Sequencing

Genomic DNA was extracted from tumors or cells using the previously published salt-precipitation protocol (11). The sgRNA library representation was determined using a two-step PCR process in which PCR1 amplifies the lentiviral sequence containing the 20 bp sgRNA cassette and PCR2 attaches Illumina sequencing adapters and barcodes. Primer sequences were obtained from the Zhang lab online resource (http://genome-engineering.org/gecko/) using v2Adaptor_F and v2Adapter_R for PCR1 and primers F01–F06 and R01–R02 for PCR2. All PCR reactions were performed using Herculase II Fusion DNA Polymerase (Agilent). Sufficient PCR1 reactions were performed to maintain library coverage. For the genome-wide screen a total of 200 μg of genomic DNA template per sample with 10 μg of gDNA per 100 μL PCR1 reaction; ≥20 PCR1 reactions per biologic sample. For the focused secondary screen a total of 18μg of genomic DNA template per sample with 6μg of gDNA per 100μL PCR1 reaction; ≥3 PCR1 reactions per biologic sample. After pooling the PCR1 product, 10 μL was used for each PCR2 reaction. PCR2 was performed with one reaction per 10^4 constructs (7 PCR2 reactions per sample). PCR products were purified and quantified with Qubit and/or Bioanalyzer and diluted libraries were sequenced on an Illumina NextSeq (TSRI core).

Data Processing and Analysis

Illumina NextSeq sequencing reads were de-multiplexed and the adapters trimmed using cutadapt to leave only the 20 bp sgRNA spacer sequences. The sgRNA spacer sequences were then mapped to the reference human GeCKO Library A using Bowtie, allowing a maximum of one mismatch and allowing only uniquely aligning reads. Only sgRNA spacers with multiple reads were analyzed (sgRNA spacers with only a single read were filtered out). Normalized read counts were obtained by normalizing to total read count per sample (normalized reads per sgRNA = reads per sgRNA/total reads for all sgRNAs in the sample × 10^6 + 1). CRISPR guide scores were generated by calculating the log fold change of normalized sgRNA read counts between xenograft samples and the baseline T0 samples. The log fold change was then normalized to the median of the non-targeting control sgRNAs for each sample. RIGER analysis was performed using GENE-E software (Broad Institute) using the weighted sum method to convert sgRNAs to genes and 1 × 10^7 number of

permutations. STARS analysis was performed using the STARS software v 1.2 (Broad Institute) with a threshold of 25 and 500–1000 iterations.

RESULTS

Genome-Wide CRISPR-Cas9 Screen of Isogenic Human Colorectal Cancer Cells Harboring Wild-Type or Mutant *KRAS*

To conduct a CRISPR-Cas9 knockout screen in an in vivo setting, we used a well-characterized isogenic pair of human CRC lines that differ only in the presence ($HCT116^{MUT}$) or absence ($HCT116^{WT}$) of an activating G13D *KRAS* mutation. These cell lines have previously been used by our lab to conduct a high-throughput screen of oncogenic *KRAS* synthetic lethal microRNAs (13). We transduced $HCT116^{WT}$ and $HCT116^{MUT}$ cells with the human GeCKO v2 library, which contains 65,383 sgRNA constructs targeting 19,050 human coding genes (3 sgRNAs per gene) and 1864 microRNAs (4 sgRNAs per gene) (8). Duplicate transductions were performed at a low MOI (0.2) to ensure transduction with only one sgRNA per cell, thereby effectively barcoding individual cells. Sufficient cell numbers (1.6×10^8 cells) were transduced to allow 500× coverage of each sgRNA within the library, and this coverage was maintained at each cell passage ($>3 \times 10^7$ cells seeded per passage). Cells were selected for stable viral integration with puromycin for 7 days and then subcutaneously injected into the flanks of nude mice (3×10^7 cells per mouse, 3 mice per duplicate cell line: total n = 12 mice). The mice were euthanized 14 days later, the tumors were excised, and genomic DNA was extracted. Lentiviral sgRNA constructs were then PCR-amplified and quantified by deep sequencing (Figure 1A). As a surrogate for cell proliferation, we analyzed enrichment or depletion of sgRNA abundance in the tumor xenografts compared with levels in the cell lines pre-injection. It was expected that sgRNAs targeting genes that are essential for tumor growth would be less abundant in the xenografts compared with the pre-injection cells, while sgRNAs targeting genes that normally control growth (i.e., tumor suppressors) would be enriched in the xenografts compared with pre-injection cells.

The majority of the pre-injection sgRNA library was recovered in the tumor samples, with 93% of the sgRNA library constructs (92% of non-targeting control sgRNAs) containing multiply aligning reads in all samples and little apparent random loss during cell injection (Figure S1A). Replicate mice from the duplicate transductions showed good correlation at the sgRNA level (Figure S1B) and gene level (Table S1). Screen performance was analyzed using previously published essential and non-essential reference gene sets (7,14) and the 1000 non-targeting control sgRNAs in the GeCKO library. We then compared the change in sgRNA representation in $HCT116^{WT}$ vs. $HCT116^{MUT}$ xenografts using the CRISPR-Cas9 guide score (15), which is the median-corrected log fold change in abundance of each sgRNA in the xenograft compared with the pre-injection cell population. Non-targeting control sgRNAs and non-essential genes clustered around the center of the plots, indicating that they were neither enriched nor depleted in either xenograft (Figure 1B). As expected, sgRNAs targeting most (92%) of the reference essential genes were depleted in both $HCT116^{WT}$ and $HCT116^{MUT}$ xenografts compared with the pre-injection cells (Figure 1B). However, consistent with previous studies, not every sgRNA in the GeCKO library was

equally efficacious, and some sgRNAs targeting essential genes were not depleted (Figure 1B).

Pathway Analysis of the In Vivo GeCKO CRISPR-Cas9 Screen Identifies Multiple Metabolic Vulnerabilities in *KRAS* Mutant Tumors

We next performed pathway analysis of sgRNAs that were commonly or selectively depleted in $HCT116^{MUT}$ vs $HCT116^{MUT}$ xenografts. Gene set enrichment analysis (GSEA) of KEGG pathways of commonly depleted sgRNAs (i.e., lethal or essential genes) identified ribosome and spliceosome components as the two most significant hits, which is consistent with the results of earlier in vitro screens (7) (Figures 1C and 1D). In contrast, pathway analysis of sgRNAs depleted in $HCT116^{MUT}$ xenografts but not in $HCT116^{WT}$ xenografts (*KRAS* synthetic lethal) revealed enrichment of genes associated with the MAPK signaling pathway and multiple metabolic pathways, including oxidative phosphorylation (Figures 1C and 1D).

For further analysis, we examined genes for which at least 2 sgRNAs were selectively depleted in $HCT116^{MUT}$ xenografts (Table S2). We applied a cutoff value of >0.5 $\log_2$ fold decrease in abundance $HCT116^{MUT}$ compared with $HCT116^{WT}$ xenografts, which effectively excluded >90% of non-targeting control sgRNAs. The gene hits defined by these criteria included previously validated targets of the MAPK signaling pathway (*MAPK1/* ERK2) and metabolic pathways (*GFPT1*) (7,16). Among the novel candidate *KRAS* synthetic lethal genes identified were metabolic genes in the tricarboxylic acid cycle (succinate-CoA ligase ADP-forming beta subunit, *SUCLA2*), pentose phosphate pathway (nicotinamide adenine dinucleotide kinase, *NADK*), and fructose metabolism (ketohexokinase, *KHK*) (Figures 2A and Table S2). Notably, these genes did not display synthetic lethality in a parallel genome-wide screen of 14 day-cultured $HCT116^{WT}$ and $HCT116^{MUT}$ cells (Figure 2A) or in other in vitro screens, including of HCT116 cells (7), substantiating the importance of recapitulating the in vivo tumor microenvironment in order to identify relevant therapeutic targets.

To validate the identified metabolic genes, we generated 2 independent sgRNAs per gene and transduced them into stable Cas9-expressing $HCT116^{WT}$ and $HCT116^{MUT}$ cell lines. The knockout cell lines were then deep sequenced to determine the CRISPR mutagenesis frequency. On-target insertions, deletions, and substitutions, most of them small, were observed for each of the sgRNAs, with similar genomic effects in $HCT116^{WT}$ and $HCT116^{MUT}$ cells (Figure S2A). Protein knockdown in the cells was also confirmed by immunohistochemistry (Figure S2B), and the cells were then injected into nude mice (n = 3–4 mice per sgRNA). Knockout of *SUCLA2*, *NADK*, and *KHK* significantly reduced the growth of $HCT116^{MUT}$ xenografts but not of $HCT116^{WT}$ xenografts (Figures 2B and 2C). As positive controls, cells were also transduced with individual *KRAS*- or *MAPK1*-targeting sgRNAs and, as expected, they selectively decreased the growth of $HCT116^{MUT}$ tumors (Figure S2C).

To verify the CRISPR knockdown results, we examined the effects on tumor growth of small molecule inhibitors of NADK and KHK (no inhibitors of SUCLA2 were available). NADK has previously been proposed as a possible therapeutic target in cancer, since NADPH is

essential to support enhanced biosynthesis and to control redox status (17) (Figure 2D). Consistent with this, administration of thionicotinamide (thioNa), a small molecule inhibitor of NADK (18), showed significant inhibition of the growth of $HCT116^{MUT}$ xenografts but not of $HCT116^{WT}$ xenografts (Figures 2E and 2F). KHK has also recently been described as a possible therapeutic target for hepatocellular carcinoma (19,20). KHK exists as two isoforms, KHK-A and KHK-C, which are generated by alternative splicing of exons 3A or 3C, respectively. KHK-C has the greater affinity for fructose and is expressed specifically in hepatocytes. KHK-A is more widely expressed and has been shown to phosphorylate phosphoribosyl pyrophosphate synthetase 1 (PRPS1), which is involved in *de novo* purine synthesis (Figure 2D). We found that KHK-A is the predominant isoform in HCT116 cells and other *KRAS* mutant cancer cell lines of different lineages (non-small-cell lung cancer [NSCLC] and PDAC; Figure S2D). We also confirmed that the 2 validation sgRNAs targeted exons 3A or 4 which would knockout KHK-A expression and that the exon 3C-targeting sgRNAs had no effect on the growth of $HCT116^{MUT}$ xenografts (Figure S2E), consistent with the predominant expression of KHK-A in these cells. To determine the effect of KHK inhibition on xenograft growth, mice were administered a commercially available small molecule KHK inhibitor (Figure 2D and S2F (12)), which binds to the conserved ATP-binding domain present in both KHK isoforms (Figure S2G). This compound significantly inhibited the growth of $HCT116^{MUT}$ xenografts, but not $HCT116^{WT}$ xenografts (Figures 2G and 2H), confirming the CRISPR knockdown data and establishing the importance of this enzyme for the growth of *KRAS* mutant tumors.

A Secondary In Vivo sgRNA Screen Identifies Candidate *KRAS*-dependent Tumor Suppressor and Synthetic Lethal Genes

We next performed a smaller focused screen with higher depth (more sgRNAs per gene) and coverage per construct (1000× coverage) to further validate the genome-wide screen and to detect hits with greater power. Recent studies subsampling large genome-wide CRISPR screens support this strategy in which a broad genome-wide screen is first performed with a limited number (3–4) of sgRNAs per gene and then relaxing the FDR threshold (75%) to generate candidates for a secondary screen of a limited number of genes with greater depth (~6 sgRNAs per gene (6).

To generate a candidate gene list for our secondary screen library, we used the RNAi Gene Enrichment Ranking (RIGER) algorithm to rank significantly depleted sgRNAs in the genome-wide screen. This method considers all sgRNAs for a gene similarly to a gene set in GSEA and takes into account the sum effect of all sgRNAs against a particular gene (21). To find candidate *KRAS* enhancing and lethal genes (i.e., targeted by sgRNAs enriched or depleted, respectively, in $HCT116^{MUT}$ xenografts), we identified genes overlapping in multiple RIGER comparisons of the isogenic paired screen (see Supplemental Experimental Procedures and Figures S3A and S3B), and finally obtained 152 candidate KRAS lethal genes and 160 candidate KRAS enhancing genes. Of note, the candidate gene lists did not completely overlap with the pathway analysis list, and the secondary library did not include the validated hits from the pathway analysis.

We then created a custom pooled sgRNA library consisting of ~2500 sgRNAs targeting 250 genes (9 sgRNAs per gene) selected from the KRAS lethal (~150 genes) and KRAS enhancing (~70 genes) candidates, sgRNAs targeting 20 essential genes, and 230 non-targeting control sgRNAs (Table S3). Analysis of the CRISPR-Cas9 guide scores from the genome-wide screen confirmed that, on average, the sgRNAs targeting the candidate KRAS lethal and enhancing genes were selectively depleted or enriched, respectively, in HCT116^{MUT} xenografts (Figure 3A).

The pooled lentiviral sgRNA libraries were generated by oligonucleotide array synthesis, transduced into HCT116^{WT} and HCT116^{MUT} cells, and screened in xenografts vs pre-injection cells in a similar manner to the genome-wide screen (Figure 3B). However, the focused screen was performed at a higher coverage of 800–1000× in triplicate transductions (3 mice per cell line, 3 transductions; total of 18 mice). Replicate mice from the triplicate transductions again showed good correlation at the sgRNA level (Figure S3C) and gene level (Table S4). Also similar to the findings with the genome-wide screen were (i) the majority of non-targeting control sgRNAs were neither enriched nor depleted in the xenografts, (ii) many of the sgRNAs targeting essential genes were depleted in both xenografts, and (iii) multiple *MAPK1*-targeting sgRNAs were selectively depleted in HCT116^{MUT} xenografts (Figures 3C and 3D). A new observation was that multiple *KRAS*-targeting sgRNAs were selectively depleted in HCT116^{MUT} xenografts, which was likely due to the increased coverage and depth of the secondary library (Figures 3C and 3D). Using the STARS algorithm (6) to rank the genes at a FDR of <5%, we found that *KRAS*, *MAPK1*, *SNRPC* (small nuclear ribonucleoprotein polypeptide C), and predicted *miR-4663* were depleted to a greater extent in HCT116^{MUT} xenografts compared with HCT116^{WT} xenografts (Figure 3E and Table S4). Relaxing the FDR cutoff to 25%, *POP5* (POP5 homolog subunit of ribonuclease P/MRP), *SF3B2* (splicing factor 3b subunit 2), and *LENG9* (leukocyte receptor cluster member 9) emerged as potential *KRAS* synthetic lethal candidates (Figures 3E and 3F). *SNRPC*, *POP5*, and *SF3B2* also scored as essential hits in the Toronto Knockout HCT116^{MUT} in vitro screen (7). Thus, our secondary screen identified previously unknown candidate *KRAS* synthetic lethal genes for future validation studies.

In addition to the depleted sgRNAs, the secondary screen identified several sgRNAs that were highly enriched in the tumor xenografts compared with pre-injection cells, suggesting that they confer a proliferation advantage in vivo and thus may be novel tumor suppressors in the context of mutant KRAS. In support of this, we found that the most highly enriched sgRNAs targeted the known tumor suppressors *NF2* and *RALGAPB*, with the HCT116^{MUT} xenografts showing enrichment of multiple sgRNAs (Figures S4A). *NF2* encodes the protein Merlin and is a regulator of Hippo signaling, which exerts tumor suppressive effects through the Wnt/β-catenin (22,23) and LIN28B–let-7 (24) pathways. *RALGAPB* encodes the regulatory subunit of the GTPase activating protein for the Ral GTPase, which is involved in signaling downstream of RAS. Loss of RalGAPβ has been shown to increase mTOR activity and its knockdown increases PDAC invasion (25).

While more enriched in HCT116^{MUT} xenografts, *NF2* and *RALGAPB* also score as the most highly enriched genes in HCT116^{WT} xenografts (Figure 4A). Using the STARS algorithm, we identified 6 genes for which sgRNAs were significantly enriched in

HCT116^{MUT} xenografts at a FDR of <5% (Figure 4B and Table S4). One of these, *INO80C,* which encodes a subunit of the conserved ATP-dependent chromatin remodeling complex INO80, scored consistently highly in HCT116^{MUT} xenografts (FDR < 8% in all 3 replicates) but not in HCT116^{WT} xenografts (bottom 75% of enriched sgRNAs). Moreover, many *INO80C*-targeting sgRNAs were enriched only in HCT116^{MUT} xenografts and ranked highly based on CRISPR guide scores (Figure 4A). These findings suggested that *INO80C* is a novel potential tumor suppressor in *KRAS*^{MUT} tumors. The potential clinical relevance of this candidate novel tumor suppressor was confirmed by interrogating PDAC datasets from The Cancer Genome Atlas (TCGA), which revealed frequent (4–18%) deep deletions of *INO80C* (Figure S4B). Moreover, analysis of additional TGCA datasets identified a significant association between *INO80C* deletion and worse prognosis in patients with *KRAS*^{MUT} CRC, NSCLC, and PDAC (Figure S4C). We tested the pooled validation library in xenografts from a *KRAS* mutant PDAC cell line (Capan-2) in replicate (n=3 mice per replicate) and confirmed that *INO80C* also enriched as a top hit (Figure 4C). We then directly tested the effect of *INO80C* knockout on tumor xenograft growth by transducing stable Cas9-expressing HCT116^{MUT} and HCT116^{WT} cells with two independent *INO80C*-targeting sgRNAs. Indeed, *INO80C* knockout significantly and selectively enhanced the growth of HCT116^{MUT} xenografts (Figures 4D and S4D). This effect was confirmed with a second pair of isogenic CRC cell lines, DLD-1-*KRAS*^{WT} and DLD-1-*KRAS*^{MUT}, although the increase in tumor growth was not as pronounced as for HCT116 xenografts (Figures 4D and S4D). Finally, we performed CRISPR knockout of *INO80C* in a *KRAS*^{MUT} PDAC cell line, Capan-2, and a KRAS^{MUT} NSCLC cell line, H348, and found significant enhancement of tumor growth (Figures 4E and S4E). Collectively, these data not only identify *INO80C* as a novel potential tumor suppressor gene but also establish its relevance in human tumors harboring mutant *KRAS*.

DISCUSSION

KRAS oncogenic mutations occur in many of the most lethal types of cancers. Despite years of study, *KRAS*^{MUT} cancers remain among the most difficult to treat, due in large part to the lack of targeted agents. There is thus a significant unmet need to develop therapies that selectively inhibit activated *KRAS* and/or its downstream effector pathways. The advent of CRISPR-Cas9–based genetic screens has dramatically improved our ability to interrogate the genome in an unbiased manner, and such screens hold great promise for extending our knowledge of genetic vulnerabilities in different oncogenic contexts. Oncogenes exert their effects through a myriad of pathways that influence not only intracellular processes but also the interaction of tumor cells with their microenvironment to overcome external checkpoints on tumorigenesis. One of the hallmarks of cancer is aberrant cell metabolism, as reflected by the Warburg effect (26). Constitutively active oncogenic *KRAS* is known to rewire the metabolic program of cancer cells to support the energetic and biosynthetic demands of continued proliferation (16). *KRAS*^{MUT} cells show increased uptake of glucose, which can be utilized to support elevated nucleotide biosynthesis (16,27). Recent studies highlight the fact that in vivo conditions such as tumor xenografts more accurately recapitulate the microenvironment associated with key metabolic phenotypes than do cell cultures, thereby facilitating the search for therapeutic targets (27).

Here, we conducted a genome-wide CRISPR-Cas9 screen of tumor xenografts formed by isogenic *KRAS*^{MUT} and *KRAS*^{WT} CRC cells to identify candidate genes that selectively enhance or inhibit tumor growth in vivo. Pathway analysis identified genetic vulnerabilities in multiple metabolic pathways, such as nucleotide synthesis and redox balance in which *NADK* and *KHK* play important roles. Genetic knockout and small molecule inhibition of these targets more potently reduced the growth of *KRAS*^{MUT} xenografts than of *KRAS*^{WT} xenografts, suggesting they may be novel therapeutic targets in *KRAS* mutant cancers.

In support of *NADK* as a cancer therapeutic target, a recent large-scale functional screen of low-frequency mutations in PDAC identified activating mutations in *NADK* that behaved as oncogenic drivers (28). NADK inhibition also inhibited the growth of a number of tumor types in vitro and in vivo (17). Activated *KRAS* maintains low intracellular levels of reactive oxygen species (ROS) while vigorously promoting metabolic activity. Thus, perturbation of these pathways to tip the redox balance may be a particularly effective treatment for *KRAS*^{MUT} tumors, as supported by the recent discovery that high doses of vitamin C selectively kill *KRAS*^{MUT} xenografts by increasing ROS that inhibit glyceraldehyde 3-phosphate dehydrogenase (GAPDH), resulting in an energetic crisis and cell death (29). Decreases in NADP/NADPH ratios activate GAPDH and enhance oxidative pentose phosphate pathway flux, which mitigates oxidative stress by increasing NADPH levels. Thus, by inhibiting the conversion of NADP to NADPH, NADK inhibition may decrease the ability of *KRAS*^{MUT} tumors to cope with oxidative stress.

KHK has also emerged as a potential therapeutic target in cancer. A recent study identified a switch from KHK-C to KHK-A isoform expression in hepatocellular carcinoma mediated by c-Myc and heterogeneous nuclear ribonucleoprotein H1/2 (19,20). This switch has two key effects: a decrease in fructose metabolism through KHK-C, which reduces ROS levels, and an increase in PRPS1 activity, which enhances nucleotide production. Both of these effects are predicted to benefit *KRAS*-mutated cancers, and fructose has also been shown to promote the growth of pancreatic cancer cells (30).

Our secondary focused screen revealed known and novel genes as potential synthetic lethal partners with *KRAS*^{MUT}. While the identification of *KRAS* and *MAPK1* was expected, the novel genes include *SNRPC*, *POP5*, *SF3B2*, *LENG9*, and predicted *miR-4663*. These targets should be validated in future studies. *SNRPC* (also known as U1C) encodes a protein component of the U1 small nuclear ribonucleoprotein involved in spliceosome formation (31) and interacts with the RNA-binding protein EWS (32,33). EWS is involved in chromosomal translocation in human cancers such as Ewing sarcoma (EWS/FL-1 fusion) and desmoplastic small round cell tumor (EWS/WT1 fusion), which are thought to promote oncogenesis by acting as transcriptional activators (34). EWS/FL-1 fusion protein has been shown to constitutively activate *MAPK1* transcription and thus MAPK signaling (35). *POP5* encodes a protein associated with RNase MRP and RNase P complexes but has no known roles in cancer (36). *SF3B2* encodes a splicing factor that has been shown to be targeted by HIV to induce cell cycle arrest (37). *LENG9* encodes an uncharacterized protein of unknown function and miR-4663 encodes a predicted but unvalidated microRNA identified by RNA sequencing from breast cancer tissue (38).

The positive-selection side of the secondary screen, which yielded a much higher signal compared to the dropout side, identified *NF2* and *RALGAPB* as potential tumor suppressor genes in both $KRAS^{WT}$ and $KRAS^{MUT}$ xenografts. Another candidate tumor suppressor in $KRAS^{MUT}$ xenografts was *INO80C,* which we also validated by demonstrating that knockout enhanced the growth of $KRAS^{MUT}$ HCT116 and DLD-1 CRC xenografts as well as $KRAS^{MUT}$ H358 NSCLC xenografts. Based on the frequent deep deletions noted in PDAC TCGA datasets, we additionally examined the effects of *INO80C* deletion in a $KRAS^{MUT}$ PDAC cell line, Capan-2, and found that it also enhanced tumor growth in vivo. While the SWI/SNF family of chromatin remodelers, which are frequently mutated or lost in many tumors including PDAC, have been more widely studied, the INO80 complex has recently been implicated in carcinogenesis (39,40). INO80 is a large multi-subunit complex that maintains genome stability through nucleosome editing, such as removal of the histone variant H2A.Z (41). In yeast, the homolog of *INO80C* (Ies6) combines with ACTR5 (Arp5) to form a complex (42) shown to be important in demarcation of transcriptional units through inhibition of H3K79 methylation (43). Intriguingly, knockout of this sub-complex in yeast alters transcription of metabolic gene networks that downregulate glycolysis and upregulate mitochondrial energy-generating processes (42). Further analysis of the role of *INO80C* in $KRAS^{MUT}$ tumors may reveal novel elements of RAS biology.

Our study demonstrates the feasibility of genome-wide pooled CRISPR-Cas9 knockout screens of tumor xenografts for uncovering genetic vulnerabilities that may be amenable to therapeutic targeting. We identified *NADK* and *KHK* as candidate metabolic gene targets that were not previously identified using in vitro screens. We also found that a smaller positive-selection screen was particularly effective in identifying candidate tumor suppressor genes such as *INO80C*.

Supplementary Material

Refer to Web version on PubMed Central for supplementary material.

Acknowledgments

Financial Support: This work was supported in part by the National Institutes of Health (CA177322). E.H.Y. was supported by the National Cancer Institute of the National Institutes of Health under Award Number T32CA121938

We thank Steve Head and the staff of the Next Generation Sequencing core facility at The Scripps Research Institute for help with deep sequencing, and members of the Rana lab for helpful discussion and advice.

References

1. Downward J. RAS Synthetic Lethal Screens Revisited: Still Seeking the Elusive Prize? Clinical Cancer Research: An Official Journal of the American Association for Cancer Research. 2015; 21:1802–09. [PubMed: 25878361]
2. Stephen AG, Esposito D, Bagni RK, McCormick F. Dragging ras back in the ring. Cancer Cell. 2014; 25:272–81. [PubMed: 24651010]
3. Cong L, Ran FA, Cox D, Lin S, Barretto R, Habib N, et al. Multiplex genome engineering using CRISPR/Cas systems. Science (New York, NY). 2013; 339:819–23.
4. Jinek M, Chylinski K, Fonfara I, Hauer M, Doudna JA, Charpentier E. A programmable dual-RNA-guided DNA endonuclease in adaptive bacterial immunity. Science (New York, NY). 2012; 337:816–21.

5. Mali P, Yang L, Esvelt KM, Aach J, Guell M, DiCarlo JE, et al. RNA-guided human genome engineering via Cas9. Science (New York, NY). 2013; 339:823–26.
6. Doench JG, Fusi N, Sullender M, Hegde M, Vaimberg EW, Donovan KF, et al. Optimized sgRNA design to maximize activity and minimize off-target effects of CRISPR-Cas9. Nature Biotechnology. 2016; 34:184–91.
7. Hart T, Chandrashekhar M, Aregger M, Steinhart Z, Brown KR, MacLeod G, et al. High-Resolution CRISPR Screens Reveal Fitness Genes and Genotype-Specific Cancer Liabilities. Cell. 2015; 163:1515–26. [PubMed: 26627737]
8. Sanjana NE, Shalem O, Zhang F. Improved vectors and genome-wide libraries for CRISPR screening. Nature Methods. 2014; 11:783–84. [PubMed: 25075903]
9. Shalem O, Sanjana NE, Hartenian E, Shi X, Scott DA, Mikkelsen TS, et al. Genome-scale CRISPR-Cas9 knockout screening in human cells. Science (New York, NY). 2014; 343:84–87.
10. Wang T, Birsoy K, Hughes NW, Krupczak KM, Post Y, Wei JJ, et al. Identification and characterization of essential genes in the human genome. Science (New York, NY). 2015; 350:1096–101.
11. Chen S, Sanjana NE, Zheng K, Shalem O, Lee K, Shi X, et al. Genome-wide CRISPR screen in a mouse model of tumor growth and metastasis. Cell. 2015; 160:1246–60. [PubMed: 25748654]
12. Maryanoff BE, O'Neill JC, McComsey DF, Yabut SC, Luci DK, Jordan AD Jr, et al. Inhibitors of Ketohexokinase: Discovery of Pyrimidinopyrimidines with Specific Substitution that Complements the ATP-Binding Site. ACS Med Chem Lett. 2011; 2(7):538–43. [PubMed: 24900346]
13. Zhou Y, Dang J, Chang KY, Yau E, Aza-Blanc P, Moscat J, et al. miR-1298 Inhibits Mutant KRAS-Driven Tumor Growth by Repressing FAK and LAMB3. Cancer Res. 2016; 76(19):5777–87. [PubMed: 27698189]
14. Hart T, Brown KR, Sircoulomb F, Rottapel R, Moffat J. Measuring error rates in genomic perturbation screens: gold standards for human functional genomics. Molecular Systems Biology. 2014; 10:733. [PubMed: 24987113]
15. Aguirre AJ, Meyers RM, Weir BA, Vazquez F, Zhang C-Z, Ben-David U, et al. Genomic Copy Number Dictates a Gene-Independent Cell Response to CRISPR/Cas9 Targeting. Cancer Discovery. 2016; 6:914–29. [PubMed: 27260156]
16. Ying H, Kimmelman AC, Lyssiotis CA, Hua S, Chu GC, Fletcher-Sananikone E, et al. Oncogenic Kras maintains pancreatic tumors through regulation of anabolic glucose metabolism. Cell. 2012; 149:656–70. [PubMed: 22541435]
17. Tedeschi PM, Bansal N, Kerrigan JE, Abali EE, Scotto KW, Bertino JR. NAD+ Kinase as a Therapeutic Target in Cancer. Clin Cancer Res. 2016; 22(21):5189–95. [PubMed: 27582489]
18. Tedeschi PM, Lin H, Gounder M, Kerrigan JE, Abali EE, Scotto K, et al. Suppression of Cytosolic NADPH Pool by Thionicotinamide Increases Oxidative Stress and Synergizes with Chemotherapy. Mol Pharmacol. 2015; 88(4):720–7. [PubMed: 26219913]
19. Li X, Qian X, Lu Z. Fructokinase A acts as a protein kinase to promote nucleotide synthesis. Cell Cycle. 2016; 15(20):2689–90. [PubMed: 27356213]
20. Li X, Qian X, Peng LX, Jiang Y, Hawke DH. A splicing switch from ketohexokinase-C to ketohexokinase-A drives hepatocellular carcinoma formation. 2016; 18(5):561–71.
21. Luo B, Cheung HW, Subramanian A, Sharifnia T, Okamoto M, Yang X, et al. Highly parallel identification of essential genes in cancer cells. Proceedings of the National Academy of Sciences. 2008; 105:20380–85.
22. Kim S, Jho E-H. Merlin, a regulator of Hippo signaling, regulates Wnt/β-catenin signaling. BMB reports. 2016; 49:357–58. [PubMed: 27345717]
23. Morrow KA, Das S, Meng E, Menezes ME, Bailey SK, Metge BJ, et al. Loss of tumor suppressor Merlin results in aberrant activation of Wnt/β-catenin signaling in cancer. Oncotarget. 2016; 7:17991–8005. [PubMed: 26908451]
24. Hikasa H, Sekido Y, Suzuki A. Merlin/NF2-Lin28B-let-7 Is a Tumor-Suppressive Pathway that Is Cell-Density Dependent and Hippo Independent. Cell Reports. 2016; 14:2950–61. [PubMed: 26997273]

25. Martin TD, Chen X-W, Kaplan REW, Saltiel AR, Walker CL, Reiner DJ, et al. Ral and Rheb GTPase activating proteins integrate mTOR and GTPase signaling in aging, autophagy, and tumor cell invasion. Molecular Cell. 2014; 53:209–20. [PubMed: 24389102]
26. Cantor JR, Sabatini DM. Cancer Cell Metabolism: One Hallmark, Many Faces. Cancer discovery. 2012; 2:881–98. [PubMed: 23009760]
27. Davidson SM, Papagiannakopoulos T, Olenchock BA, Heyman JE, Keibler MA, Luengo A, et al. Environment Impacts the Metabolic Dependencies of Ras-Driven Non-Small Cell Lung Cancer. Cell Metabolism. 2016; 23:517–28. [PubMed: 26853747]
28. Tsang YH, Dogruluk T, Tedeschi PM, Wardwell-Ozgo J, Lu H, Espitia M, et al. Functional annotation of rare gene aberration drivers of pancreatic cancer. Nature Communications. 2016; 7:10500.
29. Yun J, Mullarky E, Lu C, Bosch KN, Kavalier A, Rivera K, et al. Vitamin C selectively kills KRAS and BRAF mutant colorectal cancer cells by targeting GAPDH. Science. 2015; 350:1391–96. [PubMed: 26541605]
30. Liu H, Huang D, McArthur DL, Boros LG, Nissen N, Heaney AP. Fructose induces transketolase flux to promote pancreatic cancer growth. Cancer Res. 2010; 70(15):6368–76. [PubMed: 20647326]
31. Muto Y, Pomeranz Krummel D, Oubridge C, Hernandez H, Robinson CV, Neuhaus D, et al. The structure and biochemical properties of the human spliceosomal protein U1C. Journal of Molecular Biology. 2004; 341:185–98. [PubMed: 15312772]
32. Knoop LL, Baker SJ. The splicing factor U1C represses EWS/FLI-mediated transactivation. The Journal of Biological Chemistry. 2000; 275:24865–71. [PubMed: 10827180]
33. Ohkura N, Yaguchi H, Tsukada T, Yamaguchi K. The EWS/NOR1 fusion gene product gains a novel activity affecting pre-mRNA splicing. The Journal of Biological Chemistry. 2002; 277:535–43. [PubMed: 11673470]
34. Deneen B, Hamidi H, Denny CT. Functional analysis of the EWS/ETS target gene uridine phosphorylase. Cancer Research. 2003; 63:4268–74. [PubMed: 12874036]
35. Silvany RE, Eliazer S, Wolff NC, Ilaria RL. Interference with the constitutive activation of ERK1 and ERK2 impairs EWS/FLI-1-dependent transformation. Oncogene. 2000; 19:4523–30. [PubMed: 11002425]
36. van Eenennaam H, Lugtenberg D, Vogelzangs JH, van Venrooij WJ, Pruijn GJ. hPop5, a protein subunit of the human RNase MRP and RNase P endoribonucleases. The Journal of Biological Chemistry. 2001; 276:31635–41. [PubMed: 11413139]
37. Terada Y, Yasuda Y. Human immunodeficiency virus type 1 Vpr induces G2 checkpoint activation by interacting with the splicing factor SAP145. Mol Cell Biol. 2006; 26(21):8149–58. [PubMed: 16923959]
38. Persson H, Kvist A, Rego N, Staaf J, Vallon-Christersson J, Luts L, et al. Identification of new microRNAs in paired normal and tumor breast tissue suggests a dual role for the ERBB2/Her2 gene. Cancer Res. 2011; 71(1):78–86. [PubMed: 21199797]
39. Zhang S, Zhou B, Wang L, Li P, Bennett BD, Snyder R, et al. INO80 is required for oncogenic transcription and tumor growth in non-small cell lung cancer. Oncogene. 2016
40. Zhou B, Wang L, Zhang S, Bennett BD, He F, Zhang Y, et al. INO80 governs superenhancer-mediated oncogenic transcription and tumor growth in melanoma. Genes Dev. 2016; 30(12):1440–53. [PubMed: 27340176]
41. Segala G, Bennesch MA, Pandey DP, Hulo N, Picard D. Monoubiquitination of Histone H2B Blocks Eviction of Histone Variant H2A. Z from Inducible Enhancers Mol Cell. 2016; 64(2):334–46.
42. Yao W, King DA, Beckwith SL, Gowans GJ, Yen K, Zhou C, et al. The INO80 Complex Requires the Arp5-Ies6 Subcomplex for Chromatin Remodeling and Metabolic Regulation. Molecular and Cellular Biology. 2016; 36:979–91. [PubMed: 26755556]
43. Xue Y, Van C, Pradhan SK, Su T, Gehrke J, Kuryan BG, et al. The Ino80 complex prevents invasion of euchromatin into silent chromatin. Genes & Development. 2015; 29:350–55. [PubMed: 25691465]

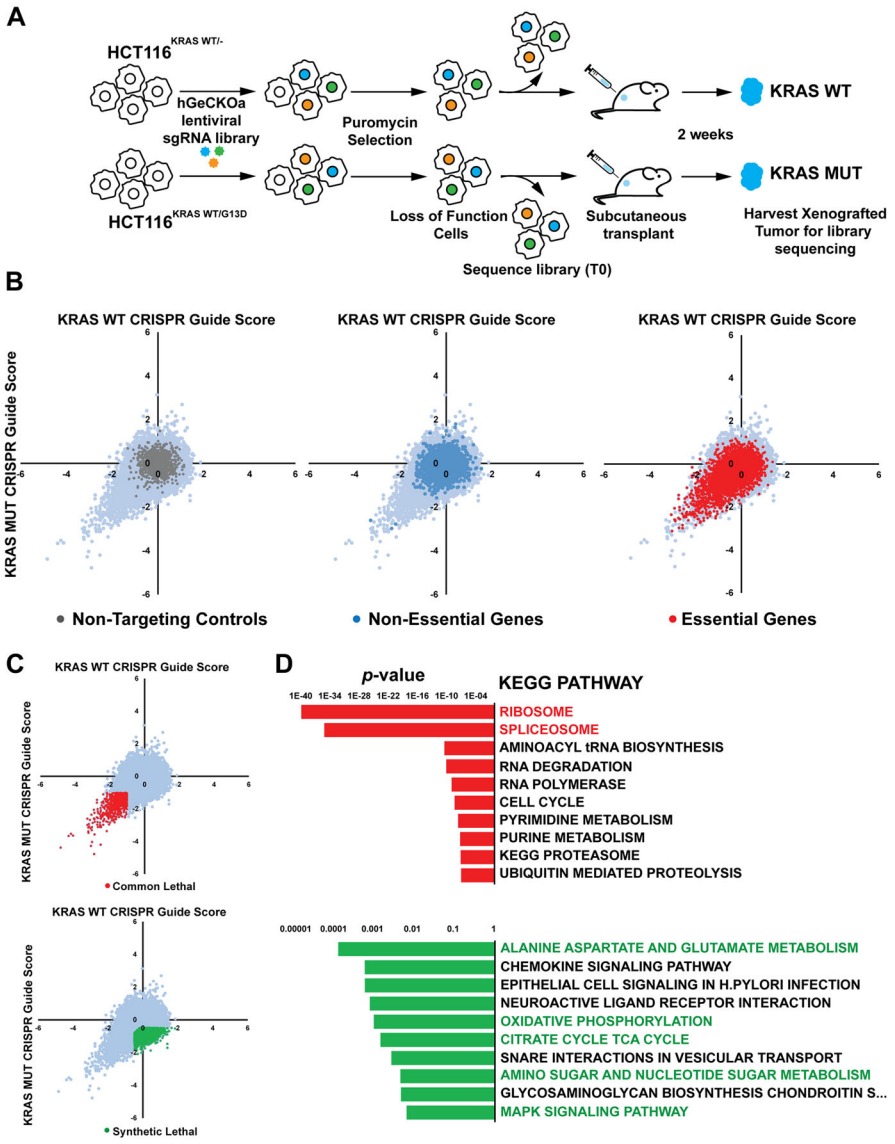

Figure 1. Genome-Wide CRISPR-Cas9 Screen of Isogenic *KRAS* WT/MUT Xenografts

(A) Schematic representation of genome-wide human GeCKO knockout screen in paired HCT116 cell lines with and without a *KRAS* G13D mutation.

(B) Scatterplots of CRISPR-Cas9 guide scores (calculated as $\log_2$ fold change of normalized read counts of individual sgRNAs in tumor xenograft samples compared with T0 cells normalized to the median $\log_2$ fold change of the non-targeting controls in each sample) for $HCT116^{WT}$ vs $HCT116^{MUT}$ xenografts. The 1000 non-targeting sgRNAs and sgRNAs against 927 reference essential genes and 1580 essential fitness genes are shown in the separate panels.

(C) Scatterplot of CRISPR-Cas9 guide scores of $HCT116^{WT}$ vs $HCT116^{MUT}$ xenografts. Common lethal sgRNAs (CRISPR-Cas9 guide score < −1 in both cell lines) are highlighted in red and *KRAS* synthetic lethal sgRNAs (CRISPR-Cas9 guide score < −0.45 in $HCT116^{MUT}$ cells, CRISPR-Cas9 guide score > −0.45 in $HCT116^{WT}$ cells, and

[$HCT116^{MUT}$ CRISPR-Cas9 guide score – $HCT116^{WT}$ CRISPR-Cas9 guide score] < −0.45) are highlighted in green.

(D) GSEA analysis of the top 10 KEGG pathways of targeted genes in the corresponding common lethal or *KRAS* synthetic lethal regions (FDR q-value threshold <0.05). Common lethal and *KRAS* synthetic lethal pathways are shown in red and green, respectively.

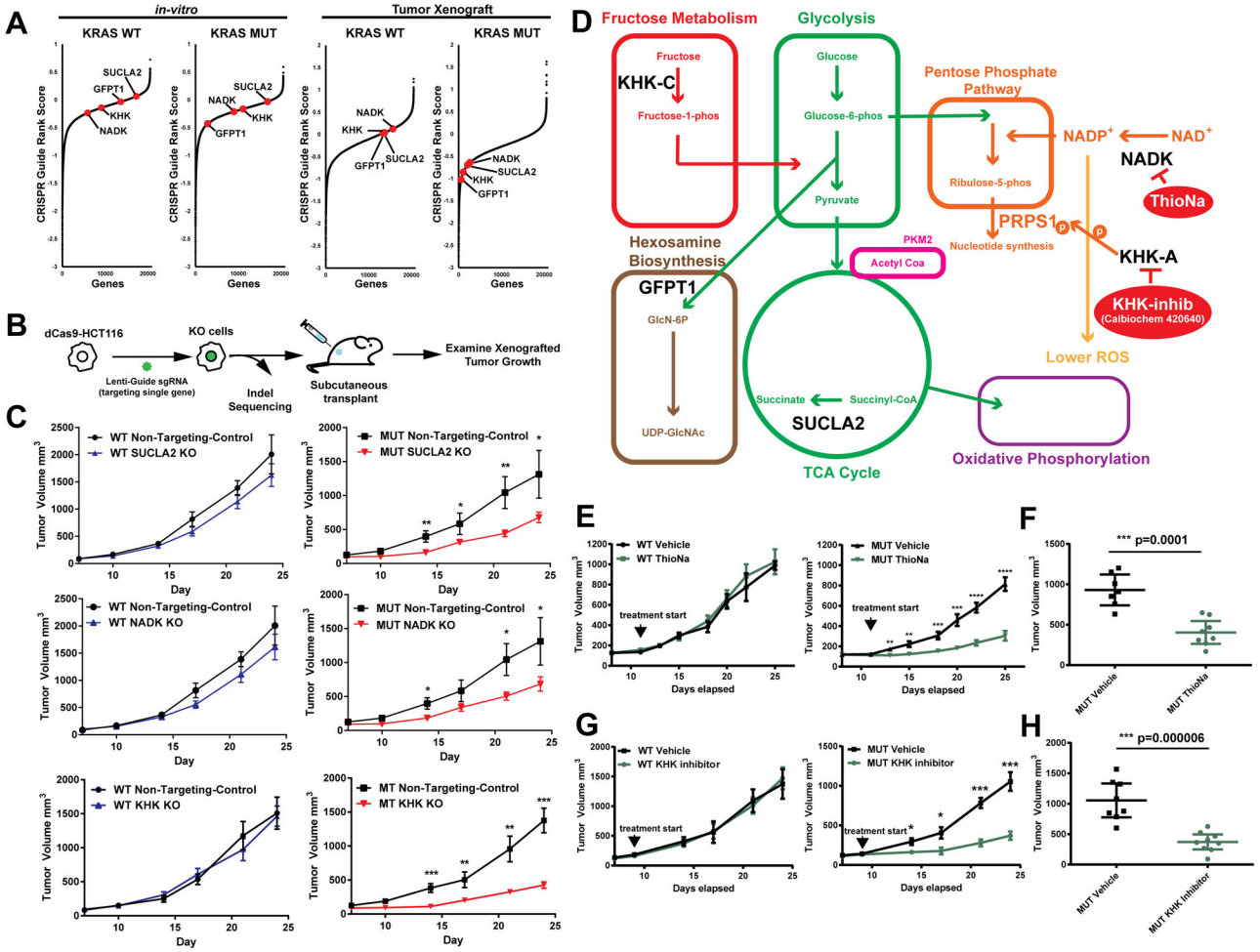

Figure 2. Validation of Individual *KRAS* Synthetic Lethal Metabolic Pathway Genes

(A) CRISPR-Cas9 guide rank score (derived from average of the two best sgRNA CRISPR-Cas9 guide scores within sgRNAs targeting a gene) for HCT116^{MUT} and HCT116^{WT} cells selected after 14 days in culture (in vitro) or after 14 days growth as tumor xenografts. Candidate genes are indicated in red.

(B) Schematic of single sgRNA tumor xenograft experiments. Stable Cas9-expressing HCT116^{MUT} or HCT116^{WT} cells were infected with single sgRNAs targeting the candidate genes, and genomic DNA was deep sequenced to analyze indels and substitutions. Cells were injected into nude mice (n = 3–4 mice per sgRNA, 2 sgRNAs; total of 6–8 mice per cell line per gene) and tumor growth was measured for 24 days.

(C) Tumor growth after injection of nude mice with HCT116^{WT} or HCT116^{MUT} cells transduced with non-targeting control sgRNAs (n = 6 mice) or *SUCLA2*-, *NADK*-, or *KHK*-targeting sgRNAs (n = 3–4 mice per sgRNA, 2 sgRNAs per gene; total of 6–8 mice per cell line per gene). Student's t-test, *p < 0.05, **p < 0.005, ***p < 0.001. Error bars indicate ± SEM.

(D) Metabolic pathways associated with genes identified in the CRISPR-Cas9 screen (*GFPT1*, *SUCLA2*, *KHK*, and *NADK*).

(E) Tumor growth after injection of nude mice with $HCT116^{WT}$ or $HCT116^{MUT}$ cells. Mice were treated with the NADK inhibitor thionicotinamide (100 mg/kg) or vehicle by intraperitoneal injection every other day between days 12 and 24 (7 doses; n = 6 or 8 mice per group for WT and MUT, respectively). Student's t-test, **p < 0.005, ***p < 0.001, ****p < 0.0001. Error bars indicate ± SEM.

(F) Tumor volumes on day 25 of the experiment shown in (E). Each symbol represents a single mouse. P value determined by Student's t-test. Bars indicate the mean and 95% confidence intervals (CIs).

(G and H) Experiments were performed as described for E and F except xenografted mice were treated with a KHK inhibitor (25 mg/kg) or vehicle (n = 8 or 9 mice per group for WT and MUT, respectively) every other day between days 8 and 21. In G, Student's t-test, **p < 0.005, ***p < 0.001, ****p < 0.0001. In G, error bars indicate ± SEM. In H, bars indicate mean and 95% CIs.

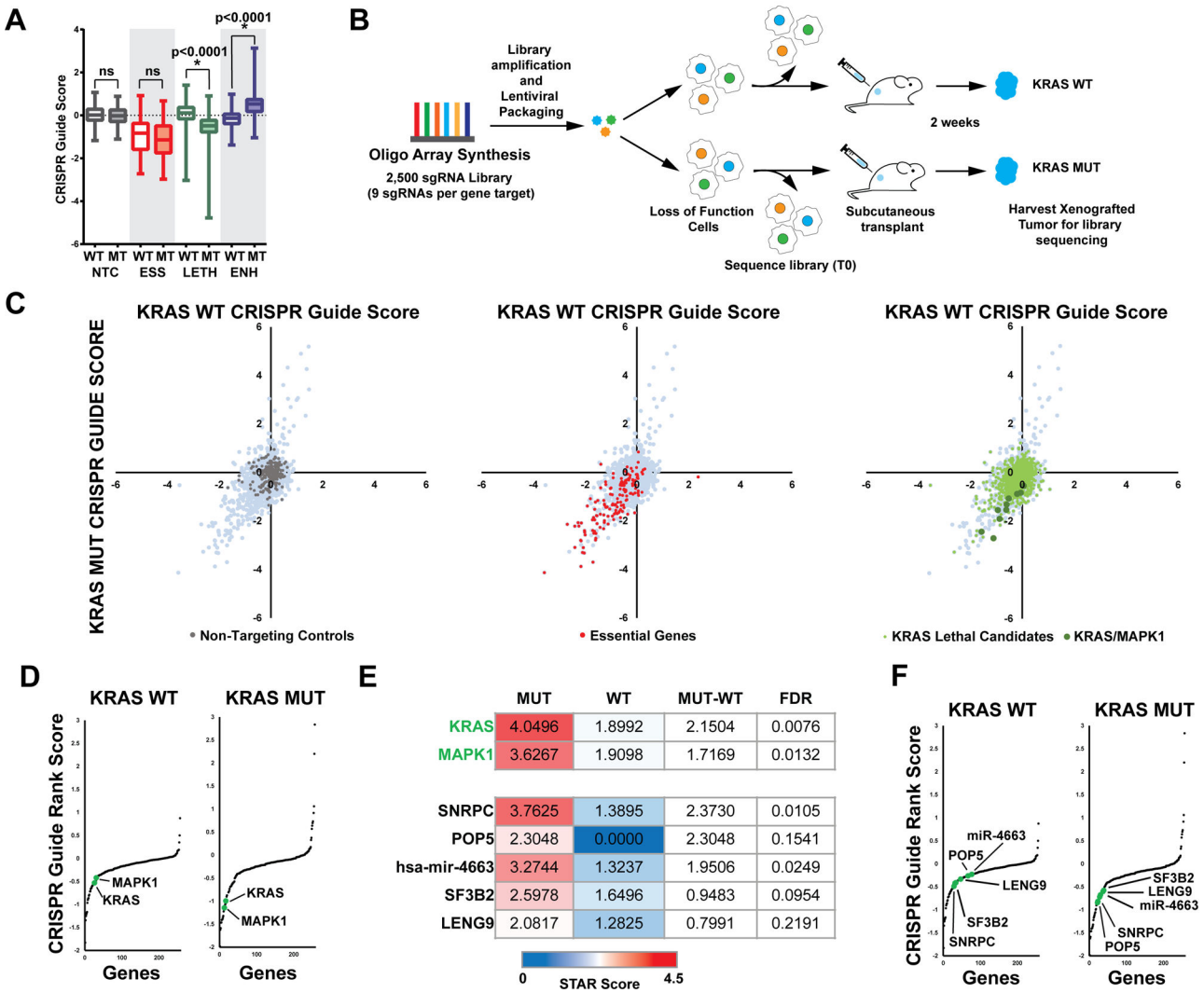

Figure 3. Focused Secondary Validation sgRNA Screen

(A) Boxplot of CRISPR-Cas9 guide scores in the primary GeCKO screen of sgRNAs targeting candidate genes selected by RIGER overlap for inclusion in the validation mini-library. P values determined by Student's t-test.

(B) Schematic of secondary mini-library screen. Lentiviruses were transfected with a pooled plasmid library representing 2500 sgRNAs targeting ~250 genes chosen from the primary GeCKO screen, with 9 sgRNAs per gene target. HCT116^{WT} and HCT116^{MUT} cell lines (n = 3) were infected with the lentiviruses and injected into nude mice (n = 3 mice per transduction replicate, total n = 18 mice).

(C) Scatterplots of CRISPR-Cas9 guide scores for HCT116^{WT} vs HCT116^{MUT} xenografts, showing 230 non-targeting control sgRNAs (gray), sgRNAs targeting 25 essential genes (red), and sgRNAs targeting 150 candidate *KRAS* lethal genes (green). Individual sgRNAs targeting *KRAS* and *MAPK1* are highlighted in dark green.

(D) CRISPR-Cas9 guide rank scores for HCT116^{MUT} and HCT116^{WT} xenografts. *KRAS* and *MAPK1* are highlighted in green.

(E) Heatmap from STAR output. Genes that scored as significantly depleted at FDR < 0.25 only in $HCT116^{MUT}$ xenografts in all 3 transduction replicates. STAR output from averaged values from 3 transduction replicates using a 25% threshold. Genes are ranked by the difference between $HCT116^{MUT}$ and $HCT116^{WT}$ STAR scores. Genes with no sgRNAs meeting the 25% threshold are given a value of 0.
(F) CRISPR-Cas9 guide rank scores for $HCT116^{MUT}$ and $HCT116^{WT}$ xenografts. Candidate *KRAS* synthetic lethal genes are highlighted in green.

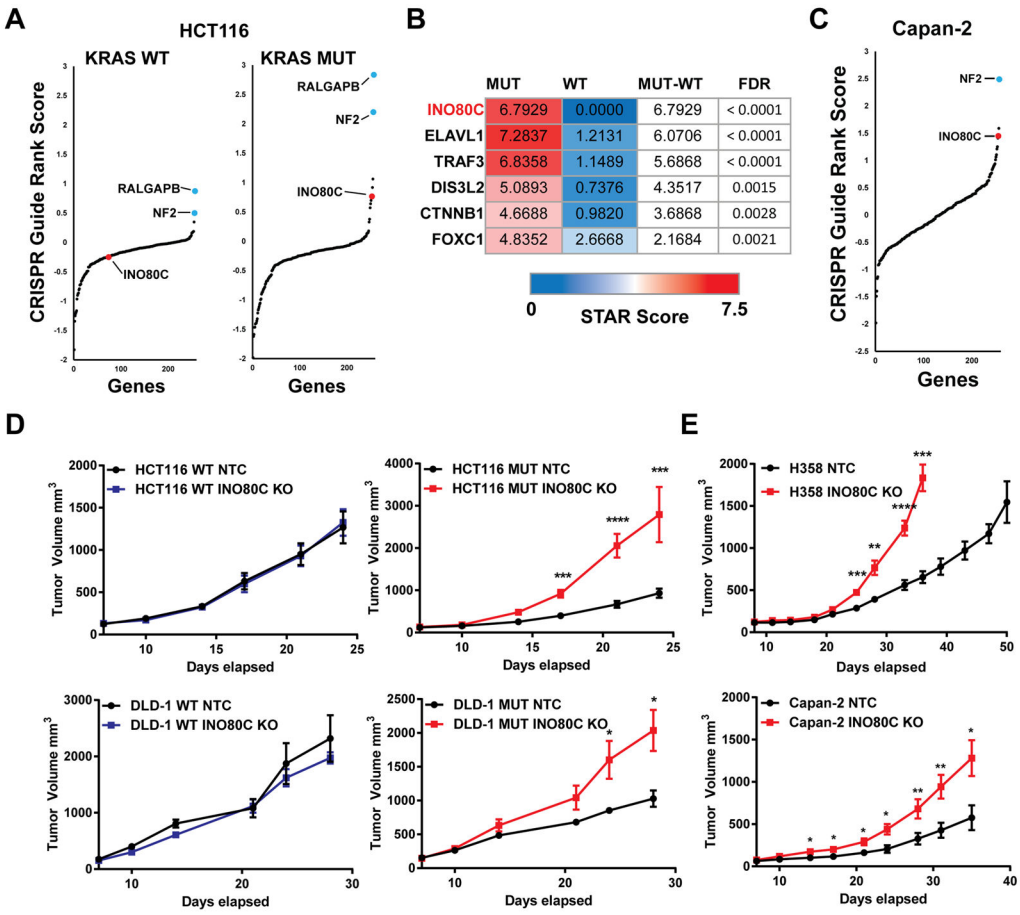

Figure 4. Identification and Validation of *INO80C* as a Candidate *KRAS*-Dependent Tumor Suppressor Gene

(A) CRISPR-Cas9 guide rank scores (derived from average of all sgRNA CRISPR-Cas9 guide scores targeting a gene) for HCT116^{MUT} and HCT116^{WT} xenografts. *INO80C*, *NF2*, and *RALGAPB* are highlighted as indicated.

(B) Heatmap from STAR output. Genes that scored as significantly enriched at FDR<0.1 only in HCT116^{MUT} xenografts in all 3 transduction replicates. STAR output from averaged values from 3 transduction replicates using a 25% threshold. Genes are ranked by the difference between HCT116^{MUT} and HCT116^{WT} STAR scores. Genes with no sgRNAs meeting the 25% threshold are given a value of 0.

(C) CRISPR-Cas9 guide rank score (derived from average of all sgRNA CRISPR-Cas9 guide scores targeting a gene) Capan-2 xenografts. *INO80C* and *NF2* are highlighted as indicated.

(D) Tumor growth after injection of nude mice with HCT116^{WT} and HCT116^{MUT} -dCas9 cells (upper) or DLD-1$^{KRAS\ WT}$ and DLD-1$^{KRAS\ MUT}$ -dCas9 cells (lower) transduced with non-targeting control sgRNAs (n = 6 mice) or *INO80C*-targeting sgRNAs (n = 4 mice per sgRNA, 2 sgRNAs per gene; total of 8 mice). Student's t-test, *p < 0.05, **p < 0.005, ***p < 0.001, ****p<0.0001. Error bars indicate ± SEM.

(E) Tumor growth after injection of nude mice with H358-dCas9 cells (upper) or Capan-2-dCas9 cells (lower) transduced with non-targeting control sgRNAs (n = 9 mice) or *INO80C*-

targeting sgRNAs (n = 5 or 6 mice per sgRNA, 2 sgRNAs; total of 11 mice). Student's t-test, *p < 0.05, **p < 0.005, ***p < 0.001, ***p<0.0001. Error bars indicate ± SEM.